Published in final edited form as:

Macromolecules. 2018 ; 51(18): .

Self-Assembly of ABC Bottlebrush Triblock Terpolymers with Evidence for Looped Backbone Conformations

Daniel F. Sunday[1], **Alice B. Chang**[2], **Christopher D. Liman**[1], **Eliot Gann**[1], **Dean M. Delongchamp**[1], **Lars Thomsen**[3], **Mark W. Matsen**[4], **Robert H. Grubbs**[2], **Christopher L. Soles**[1]

[1]Materials Science and Engineering Division, National Institute of Standards and Technology, Gaithersburg, MD 20899, United States

[2]Division of Chemistry and Chemical Engineering, California Institute of Technology, Pasadena, CA 91125, United States

[3]Australian Synchrotron, 800 Blackburn Road, Clayton, Victoria 3168, Australia

[4]Department of Chemical Engineering, Department of Physics and Astronomy, and Waterloo Institute for Nanotechnology, University of Waterloo, Waterloo, Ontario, N2L 3G1, Canada

Abstract

Bottlebrush block copolymers offer rich opportunities for the design of complex hierarchical materials. As consequences of the densely grafted molecular architecture, bottlebrush polymers can adopt highly extended backbone conformations and exhibit unique physical properties. A recent report has described the unusual phase behavior of ABC bottlebrush triblock terpolymers bearing grafted poly($_{D,L}$-lactide) (PLA), polystyrene (PS), and poly(ethylene oxide) (PEO) blocks (LSO). In this work, a combination of resonant soft X-ray reflectivity (RSoXR), near edge X-ray absorption fine structure spectroscopy (NEXAFS), and self-consistent field theory (SCFT) was used to provide insight into the phase behavior of LSO and underlying backbone chain conformations. Consistent with SCFT calculations, RSoXR measurements confirm a unique mesoscopic ACBC domain connectivity and *decreasing* lamellar periods (d_0) with increasing backbone length of the PEO block. RSoXR and NEXAFS demonstrate an additional unusual feature of brush LSO thin films: when the overall film thickness is ~3.25d_0, the film-air interface is majority PS (>80%). Since PS is the midblock, the triblocks must adopt looping configurations at the surface, despite the preference for the backbone to be extended. This result is supported by backbone concentrations calculated through SCFT, which suggest that looping midblocks are present throughout the film. Collectively, this work provides evidence for the flexibility of the bottlebrush backbone and the consequences of low-χ block copolymer design. We propose that PEO blocks localize at the PS/PLA domain interfaces in order to screen the highest-χ contacts in the system, driving the formation of loops. These insights introduce a potential route to overcome the intrinsic penalties to interfacial curvature imposed by the bottlebrush architecture, enabling the design of unique self-assembled materials.

Graphical Abstract

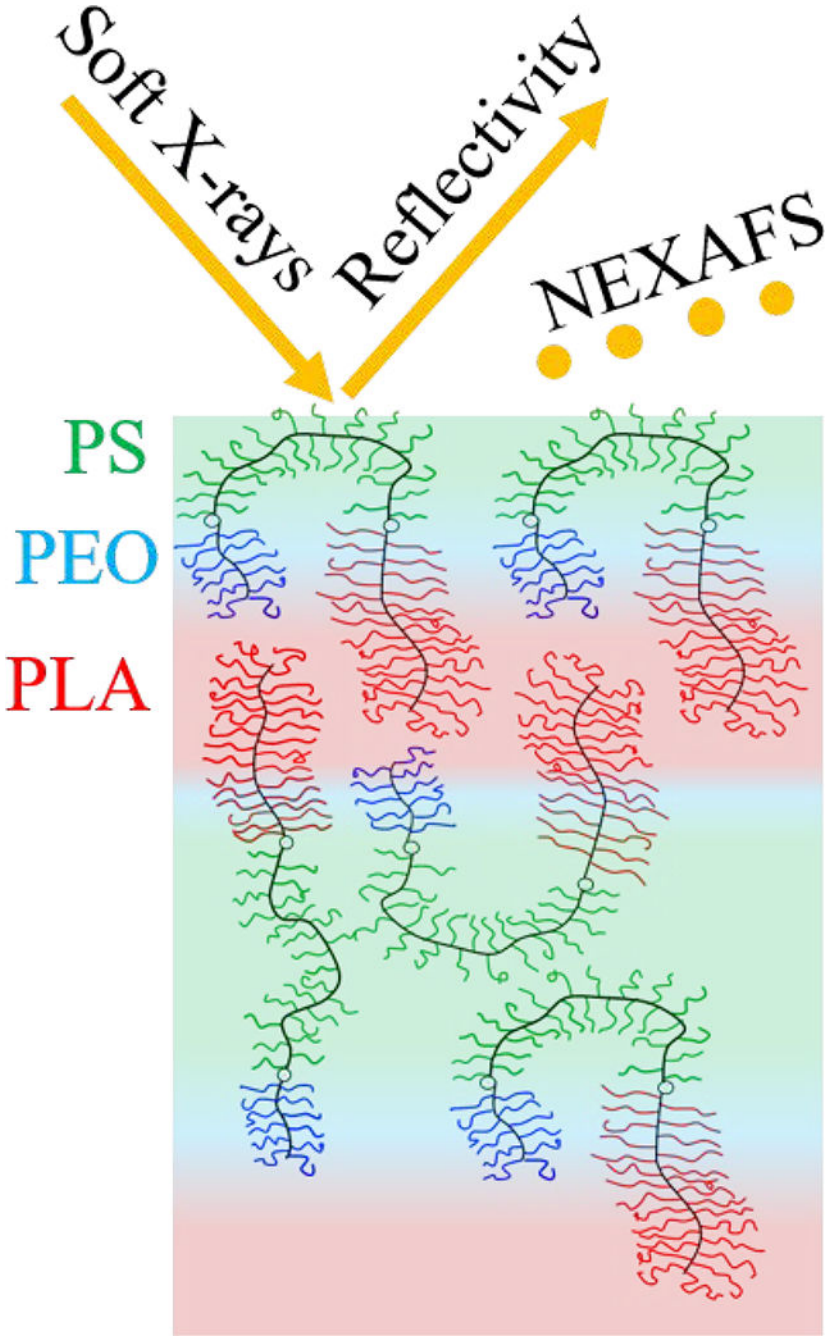

Introduction

Bottlebrush block copolymers (BCPs) are densely grafted macromolecules that feature a polymer backbone bearing polymeric side chains. Steric repulsion between the side chains imparts a certain bending rigidity to the backbone, causing bottlebrush polymers to adopt extended, wormlike conformations.[1] Due to their extended conformations, bottlebrush polymers display unique physical properties compared to linear analogues. For example, the bottlebrush architecture suppresses entanglements in the melt up to ultra-high total

molecular masses (> 1 MDa),[2–4] which facilitates fast assembly into nanostructures with ultra-large periodicities (d_0 >100 nm).[5] This ability to tune self-assembled length scales over a wide range while maintaining excellent melt processability[6] opens new opportunities to design hierarchical functional materials. Reflecting this potential, bottlebrush BCPs have found utility in a wide variety of applications, including photonics,[6,7] solid electrolytes,[8] super-soft elastomers,[9–11] biomedical materials,[12,13] and nanofabrication.[5,14,15]

Recent theoretical[16–18] and experimental[14,19,20] work provides guidance for tailoring bottlebrushes to achieve desired structures and properties. Many parameters within the enormous design space can be modified, including the side chain chemistry, grafting density (z), total backbone degree of polymerization (N_{bb}), side chain degrees of polymerization (N_{sc}), and block volume fractions (f). However, in large part due to long-standing synthetic challenges, considerable work is still needed in order to understand bottlebrush behavior ranging from the level of the backbone and side chain conformations to the factors controlling mesoscopic structure. Whereas the phase behavior of linear diblock copolymers – the simplest BCP architecture – has been extensively investigated, the phase behavior of graft BCPs remains relatively unexplored. Linear AB diblock copolymers with symmetric compositions (f_A = 1/2) typically assemble to lamellar morphologies wherein the lamellar period d_0 scales according to $d_0 \sim N^a$, where N is the total degree of polymerization and $1/2 \leq a \leq 2/3$.[21,22] The scaling exponent a reflects that the BCPs assemble with Gaussian coil-like chain conformations. For analogous graft BCPs, a is often significantly larger, reflecting the extended wormlike conformations: $d_0 \sim N_{bb}{}^{a(z)}$, where $a \sim z$.[23] In the limit of large z, a approaches 0.9, indicating that fully grafted bottlebrush BCPs are highly extended compared to linear BCPs. The backbone extension also manifests in the expanded composition window for lamellar morphologies. The steric-induced stiffening of the backbone resists interfacial curvature, discouraging the formation of higher-dimensional structures such as cylinders or spheres even at highly asymmetric compositions.[24] We note that, despite these consequences, recent theory and experiments suggest that bottlebrushes in the melt may be more flexible than generally assumed.[19,25] These results raise interesting questions about the flexibility of the bottlebrush backbone and opportunities for materials design.

A recently reported bottlebrush triblock terpolymer, featuring a polynorbornene backbone with grafted poly($_{D,L}$-lactide) (PLA), polystyrene (PS), and poly(ethylene oxide) (PEO) blocks (LSO), provides an attractive platform for studying the interplay of molecular architecture, chain conformation, and self-assembly (Figure 1).[26] Brush LSO exhibits unusual phase behavior: rather than forming the expected lamellar morphology with ABCB connectivity (LAM_3), brush LSO forms partially mixed lamellae with mesoscopic ACBC connectivity (LAM_P). Transmission electron micrographs (TEM) suggest that PEO blocks reside at the interfaces between PS and PLA domains. Furthermore, under certain conditions, d_0 *decreases* when the total molecular mass increases.[26] In order to better understand the molecular origins of this behavior, in this report we use soft X-ray techniques and self-consistent field theory to interrogate the composition distribution of brush LSO assembled in thin films.

The structure of multicomponent polymers is generally characterized using a combination of real space information, such as TEM with contrast-enhanced staining, and reciprocal space information from X-ray scattering. Both approaches are sensitive to the electron density variation in a sample, which limits the contrast in typical all-organic polymers. Soft X-ray based techniques such as resonant soft X-ray reflectivity (RSoXR)[27–29] and near edge X-ray absorption fine structure spectroscopy (NEXAFS) [30,31] are sensitive to variations in the chemical composition,[32–34] concentration[35] and bond orientation,[36,37] allowing differentiation between components that may have nearly equal electron densities in hard X-ray measurements. The soft X-ray regime (100 eV – 3000 eV) of the electromagnetic spectrum is populated by absorption edges for elements which make up the majority of organic materials, including carbon, nitrogen and oxygen. Near an atomic absorption edge, the complex index of refraction $n = 1 - \frac{\lambda^2}{2\pi}\left[\rho_R - i\rho_{Im}\right]$ (where ρ_R is the real component, ρ_{Im} is the imaginary component in terms of scattering length density (SLD) and λ is the X-ray wavelength) varies significantly as a function of energy and molecular composition due to electronic transitions between occupied and unoccupied orbitals. This sensitivity to chemical structure has been utilized to tune the contrast between the different components in soft materials, making it possible to interrogate composition distributions in sub-100 nm thick organic films.[32,38,39] While NEXAFS is primarily surface-sensitive, RSoXR has the capability to depth-profile the bonds in thin films up to several hundred nanometers thick depending on the energy, making the two techniques excellent complementary measurements for investigating thin film behavior. In this report, both RSoXR and NEXAFS were used to evaluate the composition distribution in brush LSO thin films. These measurements provide new insight into the molecular origins of the unusual phase behavior, shedding light on role of low-χ interactions and the flexibility of the bottlebrush backbone.

Materials and Methods

Sample Preparation

Brush LSO triblock terpolymers were synthesized by living grafting-through ring-opening metathesis polymerization (ROMP) according to reported procedures.[26] The molecular masses of the PLA, PS, and PEO side chains were fixed at 4.4 kg/mol, 2.3 kg/mol, and 2.0 kg/mol, respectively. A series of LSO samples was synthesized from a parent LS diblock copolymer having backbone degrees of polymerization $N_{bb,L} = 26$ and $N_{bb,S} = 24$ through the PLA and PS blocks, respectively. PEO blocks with backbone degree of polymerization $N_{bb,O} = 8$, 12, 16, and 12 were installed, varying the volume fraction of PEO from $f_{PEO} = 0.09$ to 0.20. Molecular characterization data are summarized in Table 1. The LSO samples were self-assembled on a silicon wafer with the lamellae oriented parallel to the substrate by spin coating from propylene glycol methyl ether acetate (PGMEA) (30 mg/mL, 1000 rpm). The film thickness was tuned until no island/hole formation was observed by atomic force microscopy (AFM). We note that no evidence of crystallization was observed on the timescale of sample preparation and measurement, consistent with previous reports of densely grafted PEO-containing bottlebrush BCPs.[8,26]

Resonant Soft X-Ray Reflectivity (RSoXR) and Near Edge X-Ray Atomic Fine Structure Spectroscopy (NEXAFS)

RSoXR measurements were conducted at beamline 6.3.2 at the Advanced Light Source at Lawrence Berkeley National Laboratory. Measurements at the carbon edge (270 eV – 300 eV) used a 600 mm^{-1} grating, titanium filter, nickel order sorter, and a combination of photodiode and CEM Burle detectors. The data was fit using the refl1d program, which utilizes the matrix method to calculate the simulated reflectivity profile, and uncertainties were determined using the differential evolution adaptive Metropolis (DREAM) algorithm. All uncertainties represent 95% confidence intervals. NEXAFS measurements were collected at the SXR beamline[40] of the Australian Synchrotron and corrected and normalized with the “quick as NEXAFS tool” (QANT).[41]

Self-Consistent Field Theory (SCFT)

We employ the same SCFT that was previously introduced for AB bottlebrushes[19] and later extended to the current ABC bottlebrushes.[26] The calculation models the backbone as a semi-flexible wormlike chain and the grafts as flexible Gaussian chains. The original study[19] obtained the persistence length of the backbone by fitting the equilibrium period of the lamellar phase obtained by SCFT to that of experiment. Here, we use the same persistent length of 3.1 nm, which equates to 5 backbone units. The interactions between the three types of grafts are controlled by the usual Flory-Huggins interaction parameters, which were estimated to be $\chi_{LS} = 0.08$, $\chi_{SO} = 0.049$ and $\chi_{LO} = -0.01$ based on previous experiments.[26] The spacing of the grafts is assumed to be sufficiently close to prevent other chains from interacting with the backbone. This implies that the backbone interactions remain relatively constant, and thus they are ignored in the calculation. For further simplicity, the volume of the backbone is also ignored. Using standard techniques,[42] the SCFT of this model is solved for a bulk lamellar morphology in the incompressible limit, with the equilibrium period (d_0) determined by minimization of the free energy (F).

Results and Discussion

Reflectivity measurements were conducted near the carbon edge to vary the contrast between the three components (PLA, PS, and PEO) in the LSO films and characterize their distribution. The experimental and simulated reflectivity curves for LSO-12 ($N_{bb,O} = 12$) are shown in Figure 2A. Measurements were conducted at (1) 270 eV, which is effectively non-resonant and sensitive to the electron density distribution; (2) 284 eV, which is just below the absorption peak for aromatic carbons (≈ 285 eV) and therefore sensitive to the concentration of PS; and (3) 286 eV, which is below the absorption peak for carbonyl bonds (≈ 288 eV) and sensitive to the concentration of PLA. These three energies enable considerable variation of the optical constants in the system and effective determination of the component distributions. NEXAFS measurements were used to evaluate the optical constants of bottlebrush homopolymers for each component to aid in correlating a measured SLD with the chemical composition (shown in Supporting Information [SI]).

The ρ_R profile, determined from fits to the experimental data, is shown in Figure 2B for all three energies. Several models were tested while fitting the RSoXR data. First, an ABCBA-

type model with a PEO layer isolated between PS layers was tested, representing the conventional LAM_3 morphology expected for triblock terpolymers. The LAM_3 model failed to fit the experimental data, eliminating the possibility that the material may organize differently in a thin film compared to the bulk. This comparison also evaluates the possibility that chain pull-out impacts the component distribution and periodicity, as has been previously proposed by analogy to linear ABA' triblock copolymers.[26] In linear ABA' triblocks, when the end blocks are sufficiently asymmetric, the shorter A blocks can pull out of A domains and segregate to the center of B domains, thereby increasing d_0. The reduction in free energy due to relaxation of the B blocks outweighs the enthalpic penalty to A/B mixing.[43,44] At 284 eV, RSoXR provides significant contrast between PS and PEO as a result of the sensitivity of the soft X-rays to the aromatic rings in PS; the 1s $\rightarrow \pi^*$ transition occurs around 285 eV. The presence of even a small amount of PEO in the PS domains would cause an observable change in the reflectivity profile. However, no evidence for PEO in PS domains was observed in any of the brush LSO thin films, suggesting that chain pull-out does not explain the unusual trend in d_0.

Two other models, consistent with LAM_P, were also considered. The first model assumes an *explicit* PEO layer residing at the interface between PS and PLA domains, and the second model incorporates an *implicit* PEO layer between PS and PLA domains. The best fits for both models reduced to identical SLD profiles where the PEO layer could not be explicitly observed, indicating that the bilayer model accurately captures the measured SLD profile. Based on the fits, LSO-12 forms a lamellar morphology with a PS layer at the top surface followed by alternating domains of PS and PLA with PEO at the interfaces. Near the silicon substrate, the layers become less distinct and the interfaces become broader, potentially due to restricted motion at that surface.

SCFT calculations provide further insight into the reflectivity results. The bottom half of the inset in Figure 2B shows the SCFT composition profile calculated for LSO-12. SCFT predicts that PEO will be primarily localized at the PLA/PS interfaces, with a small fraction distributed throughout the PLA layer, consistent with the partially mixed LAM_P morphology. The composition profile from the SCFT calculations can be used to calculate an SLD profile using the known values of the optical constants for each polymer at each energy. These SLD profiles derived from the SCFT simulations show excellent agreement with the experimental results, providing further support for the component distributions determined by RSoXR.

The overall changes in d_0 with $N_{bb,O}$ determined by RSoXR correspond with the d_0 values determined from small angle X-ray scattering (SAXS) measurements on the same materials in the bulk (Table 2).[26] In addition to this information, reflectivity provides a unique, powerful advantage over SAXS: the absolute thicknesses of individual domains can be directly interrogated, providing new insight into the connections between the molecular architecture and the mesoscale domain structure. With increasing $N_{bb,O}$, the mixed PLA/PEO domains maintain the same thickness $d_{L+O} \approx 16.8$ nm, while the thickness of the PS domains (d_S) decreases from 9.4 nm (LSO-8) to 6.5 nm (LSO-20). At the same time, the interfacial width (w) increases from 3.8 nm to 7.5 nm. The interface between layers in the model is described by an error function, and w is calculated from the width of the error

function (σ) according to the following relationship: $w = \sigma\sqrt{2\pi}$. The combination of these trends suggests that compatibilization of PS and PLA at the interface is the primary driver of the unusual decrease in d_0 with increasing total molecular mass. Blending at the interface screens the unfavorable high-χ interactions between PS and PLA, encouraged by the morphological frustration ($\chi_{LS} >> \chi_{LO}$) and enabled by low χ between the PLA and PEO end blocks ($\chi_{LO} \lesssim 0$).

The interfacial compatibilization also involves changes to the average cross-sectional area per chain: as increasingly long PEO blocks are localized at the interface between domains, the average distance between block-block junctions (a_{ij}) must increase. In order to maintain uniform melt density, d_0 – the orthogonal dimension – must *decrease* (Figure 3).[46,47] This change in the cross-sectional area at the interface would typically reduce both d_{L+O} and d_S,[48] but it is offset here by the increasingly long PEO blocks anchored in the PLA-rich domains. The correspondence between the thin film period determined by reflectivity and the bulk period from SAXS measurements indicate that this behavior is likely consistent in both the thin film and bulk.

Figure 3 illustrates both bridging and looping midblocks, motivated by analogies to linear ABA' triblock copolymers. Both LSO and ABA' triblocks feature low-χ interactions between the end blocks ($\chi_{AC} \lesssim 0$, $\chi_{AA'} \approx 0$). Linear ABA' triblock copolymers are exhibited to exhibit end block mixing with a high fraction of looping midblocks (≥ 60%).[49,50] For brush LSO however, the presence of looping configurations (which require significant backbone curvature) may initially seem incompatible with the steric-induced stiffening of bottlebrush polymers, the SLD and SCFT profiles calculated herein address this potential conflict. One intriguing result that sheds light on the behavior of these materials is the presence of the PS block at the air interface (Figure 2B). In order to confirm the composition at the surface, NEXAFS measurements around the carbon edge were conducted on LSO-12 (Figure 4). NEXAFS is exquisitely sensitive to the chemical composition within the first five nanometers of the surface. The LSO-12 NEXAFS spectra show a strong absorption peak around 285 eV, which corresponds to the 1s→π* transition for the aromatic rings in polystyrene. A second distinct peak is observed around 288 eV, which corresponds to the 1s→π* transition for the carbonyl bond in PLA. (A small peak at 288 eV is also present at this position in the homo-PS bottlebrush reference sample due to the imide linkages in the backbone of the brush and the methyl ester end group on the PS side chain.) A quantitative fitting of the LSO-12 spectra results suggests that there is ~80 % by volume of PS at the top surface, consistent with the findings of the RSoXR measurements. Given that NEXAFS is sensitive to several nanometers beneath the top surface, some or all of the PLA and PEO in the signal likely originates from the components beneath the PS layer. As shown in the SI (Figures S2–S4), RSoXR measurements demonstrate that PS appears at the top surface for all four samples measured ($N_{bb,O}$ = 8, 12, 16, 20), although the NEXAFS measurement was only performed on LSO-12 for confirmation.

Because PS comprises the midblock of brush LSO, the backbone *must* form loops, despite the conformational and packing challenges this poses for the backbone and side chains. In fact, the composition of the surface layer and small thickness relative to a fully extended chain suggest that the surface layer is composed almost entirely of looped chains. The free

energy penalty from these conformational effects is clearly outweighed by the enthalpic preference due to the mixing of PLA and PEO at the interface. Informed SCFT calculations provide further evidence for backbone curvature and the formation of looped configurations. In addition to predicting the distribution of the side chains, SCFT calculations also show the change in the backbone concentration throughout a single period (Figure 5). At the center of the PS lamella, the backbone concentration drops significantly, then increases near the PS/PLA interfaces. This behavior is consistent with a high fraction of the blocks forming loops, which result in the decrease in backbone concentration at the center of the PS block where the space is instead occupied by the side chains. We note that the persistence length for the backbone of a brush LS polymer with identical grafting density and similar sidechain molecular mass to the materials in this study was determined to be ~3.1 nm.[19] By comparison, the persistence length of linear PS is ~ 1 nm.[51] While the polynorbornene backbone is clearly more rigid than most linear polymers, in this case the midblock is long enough (~5 persistence lengths) to be considered flexible and have nearly equal probability of forming loops and bridges. Any ABA' polymer is expected to form loops under the condition that the contour length of the midblock is greater than the persistence length, and the same criteria are expected to determine whether loop formation occurs in LAM_P-forming ABC systems.

The localization of PS at the air interface is interesting given that the surface free energy of PLA is slightly lower than PS (40.7 mJ/m^2 vs 41.7 mJ/m^2).[52] The intuitive configuration would be for the block with the lowest surface energy to reside at the top of the film, a behavior which is demonstrated repeatedly in linear BCP surface studies.[53] However, the brush LSO samples defy this expectation. Furthermore, unlike typical linear BCP systems, for which parallel lamellae exclusively form at film thicknesses of either half-integer multiples of d_0 (asymmetric wetting conditions) or full-integer multiples of d_0 (symmetric wetting conditions), brush LSO assembled at ~ $3.25d_0$. It is possible that a different film thickness could result in a PLA layer at the top surface, which would provide a second set of conditions which lead to the assembly of substrate-parallel lamellae. Further studies are underway to better understand the thin-film assembly of these intriguing materials.

Conclusions

Soft X-ray measurements demonstrate that bottlebrush BCPs can display a surprising degree of flexibility and shed new light on the assembly of ABC triblock terpolymers. A combination of RSoXR and NEXAFS demonstrate that, under certain conditions, the midblock in a bottlebrush triblock terpolymer is largely present at the air interface, providing evidence that the bottlebrush polymer forms loops despite the steric-induced stiffening of the backbone. SCFT calculations provide evidence that this behavior occurs throughout the film, rather than solely at the top surface. This result demonstrates a certain universality in the configurations of both linear and bottlebrush triblocks and raises interesting questions about *how* the side chains pack in looping brush midblocks and under what conditions curvature is allowed by the densely grafted polymer architecture. In linear BCPs, the ratio of looping and bridging blocks significantly impacts the mechanical performance and other physical properties.[54] Further studies will explore how the midblock configuration influences the properties of bottlebrush BCPs. We also note that bottlebrushes intrinsically resist interfacial

curvature and as a result, typically only lamellar morphologies are observed for bottlebrush BCPs with symmetric side chains. The ability of the backbone to curve presents the potential to use low-χ design to drive the assembly of high-curvature phases. Improving understanding of these phenomena will enable bottlebrush polymers to be better tailored for their many diverse applications.

Supplementary Material

Refer to Web version on PubMed Central for supplementary material.

Acknowledgements

The Advanced Light Source is supported by the Director, Office of Science, Office of Basic Energy Sciences, of the U.S. Department of Energy under Contract No. DE-AC02-05CH11231. We thank Eric Gullikson for assistance at BL. 6.3.2. This research was undertaken on the SXR beamline at the Australian Synchrotron, part of ANSTO. This work was supported by the National Science Foundation under award number CHE-1502616. A.B.C. thanks the U.S. Department of Defense for support through the NDSEG Fellowship.

References

(1). Fredrickson GH Surfactant-Induced Lyotropic Behavior of Flexible Polymer Solutions. Macromolecules 1993, 26 (11), 2825–2831.

(2). López-Barrón CR; Brant P; Eberle APR; Crowther DJ Linear Rheology and Structure of Molecular Bottlebrushes with Short Side Chains. J. Rheol 2015, 59 (3), 865–883.

(3). Dalsin SJ; Hillmyer MA; Bates FS Linear Rheology of Polyolefin-Based Bottlebrush Polymers. Macromolecules 2015, 48 (13), 4680–4691.

(4). Haugan IN; Maher MJ; Chang AB; Lin T-P; Grubbs RH; Hillmyer MA; Bates FS Consequences of Grafting Density on the Linear Viscoelastic Behavior of Graft Polymers. ACS Macro Lett. 2018, 7 (5), 525–530.

(5). Gu W; Huh J; Hong SW; Sveinbjornsson BR; Park C; Grubbs RH; Russell TP Self-Assembly of Symmetric Brush Diblock Copolymers. ACS Nano 2013, 7 (3), 2551–2558. [PubMed: 23368902]

(6). Macfarlane RJ; Kim B; Lee B; Weitekamp RA; Bates CM; Lee SF; Chang AB; Delaney KT; Fredrickson GH; Atwater HA; et al. Improving Brush Polymer Infrared One-Dimensional Photonic Crystals via Linear Polymer Additives. J. Am. Chem. Soc 2014, 136 (50), 17374–17377. [PubMed: 25373000]

(7). Sveinbjörnsson BR; Weitekamp RA; Miyake GM; Xia Y; Atwater HA; Grubbs RH Rapid Self-Assembly of Brush Block Copolymers to Photonic Crystals. Proc. Natl. Acad. Sci 2012, 109 (36), 14332–14336. [PubMed: 22912408]

(8). Bates CM; Chang AB; Momčilović N; Jones SC; Grubbs RH ABA Triblock Brush Polymers: Synthesis, Self-Assembly, Conductivity, and Rheological Properties. Macromolecules 2015, 48 (14), 4967–4973.

(9). Daniel WFM; Burdyńska J; Vatankhah-Varnoosfaderani M; Matyjaszewski K; Paturej J; Rubinstein M; Dobrynin AV; Sheiko SS Solvent-Free, Supersoft and Superelastic Bottlebrush Melts and Networks. Nat. Mater 2016, 15 (2), 183–189. [PubMed: 26618886]

(10). Sarapas JM; Chan EP; Rettner EM; Beers KL Compressing and Swelling To Study the Structure of Extremely Soft Bottlebrush Networks Prepared by ROMP. Macromolecules 2018, 51 (6), 2359–2366.

(11). Vatankhah-Varnosfaderani M; Keith AN; Cong Y; Liang H; Rosenthal M; Sztucki M; Clair C; Magonov S; Ivanov DA; Dobrynin AV; et al. Chameleon-like Elastomers with Molecularly Encoded Strain-Adaptive Stiffening and Coloration. Science 2018, 359, 1509–1513. [PubMed: 29599240]

(12). Johnson JA; Lu YY; Burts AO; Xia Y; Durrell AC; Tirrell DA; Grubbs RH Drug-Loaded, Bivalent-Bottle-Brush Polymers by Graft-through ROMP. Macromolecules 2010, 43 (24), 10326–10335. [PubMed: 21532937]

(13). Sowers MA; McCombs JR; Wang Y; Paletta JT; Morton SW; Dreaden EC; Boska MD; Ottaviani MF; Hammond PT; Rajca A; et al. Redox-Responsive Branched-Bottlebrush Polymers for in Vivo MRI and Fluorescence Imaging. Nat. Commun 2014, 5 (1).

(14). Hong SW; Gu W; Huh J; Sveinbjornsson BR; Jeong G; Grubbs RH; Russell TP On the Self-Assembly of Brush Block Copolymers in Thin Films. ACS Nano 2013, 7 (11), 9684–9692. [PubMed: 24156297]

(15). Sun G; Cho S; Clark C; Verkhoturov SV; Eller MJ; Li A; Pavía-Jiménez A; Schweikert EA; Thackeray JW; Trefonas P; et al. Nanoscopic Cylindrical Dual Concentric and Lengthwise Block Brush Terpolymers as Covalent Preassembled High-Resolution and High-Sensitivity Negative-Tone Photoresist Materials. J. Am. Chem. Soc 2013, 135 (11), 4203–4206. [PubMed: 23480169]

(16). Liang H; Cao Z; Wang Z; Sheiko SS; Dobrynin AV Combs and Bottlebrushes in a Melt. Macromolecules 2017, 50 (8), 3430–3437.

(17). Paturej J; Sheiko SS; Panyukov S; Rubinstein M Molecular Structure of Bottlebrush Polymers in Melts. Sci. Adv 2016, 2 (11), e1601478. [PubMed: 28861466]

(18). Chremos A; Theodorakis PE Morphologies of Bottle-Brush Block Copolymers. ACS Macro Lett. 2014, 3 (10), 1096–1100.

(19). Dalsin SJ; Rions-Maehren TG; Beam MD; Bates FS; Hillmyer MA; Matsen MW Bottlebrush Block Polymers: Quantitative Theory and Experiments. ACS Nano 2015, 9 (12), 12233–12245. [PubMed: 26544636]

(20). Verduzco R; Li X; Pesek SL; Stein GE Structure, Function, Self-Assembly, and Applications of Bottlebrush Copolymers. Chem Soc Rev 2015, 44 (8), 2405–2420. [PubMed: 25688538]

(21). Almdal K; Rosedale JH; Bates FS; Wignall GD; Fredrickson GH Gaussian-to Stretched-Coil Transition in Block Copolymer Melts. Phys. Rev. Lett 1990, 65 (9), 1112. [PubMed: 10043108]

(22). Matsen MW; Bates FS Unifying Weak-and Strong-Segregation Block Copolymer Theories. Macromolecules 1996, 29 (4), 1091–1098.

(23). Lin T-P; Chang AB; Luo S-X; Chen H-Y; Lee B; Grubbs RH Effects of Grafting Density on Block Polymer Self-Assembly: From Linear to Bottlebrush. ACS Nano 2017.

(24). Gai Y; Song D-P; Yavitt BM; Watkins JJ Polystyrene- Block -Poly(Ethylene Oxide) Bottlebrush Block Copolymer Morphology Transitions: Influence of Side Chain Length and Volume Fraction. Macromolecules 2017, 50 (4), 1503–1511.

(25). Cao Z; Carrillo J-MY; Sheiko SS; Dobrynin AV Computer Simulations of Bottle Brushes: From Melts to Soft Networks. Macromolecules 2015, 48 (14), 5006–5015.

(26). Chang AB; Bates CM; Lee B; Garland CM; Jones SC; Spencer RKW; Matsen MW; Grubbs RH Manipulating the ABCs of Self-Assembly via Low-χ Block Polymer Design. Proc. Natl. Acad. Sci 2017, 114 (25), 6462–6467. [PubMed: 28588139]

(27). Wang C; Araki T; Ade H Soft X-Ray Resonant Reflectivity of Low-Z Material Thin Films. Appl. Phys. Lett 2005, 87 (21), 214109.

(28). Sunday DF; Kline RJ Reducing Block Copolymer Interfacial Widths through Polymer Additives. Macromolecules 2015, 48 (3), 679–686.

(29). Sunday DF; Maher MJ; Hannon AF; Liman CD; Tein S; Blachut G; Asano Y; Ellison CJ; Willson CG; Kline RJ Characterizing the Interface Scaling of High χ Block Copolymers near the Order–Disorder Transition. Macromolecules 2018, 51 (1), 173–180. [PubMed: 29706666]

(30). Rosenberg RA; Love PJ; Rehn V Polarization-Dependent C (K) near-Edge x-Ray-Absorption Fine Structure of Graphite. Phys. Rev. B 1986, 33 (6), 4034.

(31). Patel SN; Su GM; Luo C; Wang M; Perez LA; Fischer DA; Prendergast D; Bazan GC; Heeger AJ; Chabinyc ML; et al. NEXAFS Spectroscopy Reveals the Molecular Orientation in Blade-Coated Pyridal[2,1,3]Thiadiazole-Containing Conjugated Polymer Thin Films. Macromolecules 2015, 48 (18), 6606–6616.

(32). Ferron T; Pope M; Collins BA Spectral Analysis for Resonant Soft X-Ray Scattering Enables Measurement of Interfacial Width in 3D Organic Nanostructures. Phys. Rev. Lett 2017, 119 (16).

(33). Wang C; Lee DH; Hexemer A; Kim MI; Zhao W; Hasegawa H; Ade H; Russell TP Defining the Nanostructured Morphology of Triblock Copolymers Using Resonant Soft X-Ray Scattering. Nano Lett. 2011, 11 (9), 3906–3911. [PubMed: 21805981]

(34). Salamończyk M; Vaupotič N; Pociecha D; Wang C; Zhu C; Gorecka E Structure of Nanoscale-Pitch Helical Phases: Blue Phase and Twist-Bend Nematic Phase Resolved by Resonant Soft X-Ray Scattering. Soft Matter 2017, 13 (38), 6694–6699. [PubMed: 28871294]

(35). Sunday DF; Chan EP; Orski SV; Nieuwendaal RC; Stafford CM Functional Group Quantification of Polymer Nanomembranes with Soft X-Rays. Phys. Rev. Mater 2018, 2 (3).

(36). Collins BA; Cochran JE; Yan H; Gann E; Hub C; Fink R; Wang C; Schuettfort T; McNeill CR; Chabinyc ML; et al. Polarized X-Ray Scattering Reveals Non-Crystalline Orientational Ordering in Organic Films. Nat. Mater 2012, 11 (6), 536–543. [PubMed: 22504534]

(37). Pasquali L; Mukherjee S; Terzi F; Giglia A; Mahne N; Koshmak K; Esaulov V; Toccafondi C; Canepa M; Nannarone S Structural and Electronic Properties of Anisotropic Ultrathin Organic Films from Dichroic Resonant Soft X-Ray Reflectivity. Phys. Rev. B 2014, 89 (4).

(38). Virgili JM; Tao Y; Kortright JB; Balsara NP; Segalman RA Analysis of Order Formation in Block Copolymer Thin Films Using Resonant Soft X-Ray Scattering. Macromolecules 2007, 40 (6), 2092–2099.

(39). Sunday DF; Hammond MR; Wang C; Wu W; Delongchamp DM; Tjio M; Cheng JY; Kline RJ; Pitera JW Determination of the Internal Morphology of Nanostructures Patterned by Directed Self Assembly. ACS Nano 2014, 8 (8), 8426–8437. [PubMed: 25075449]

(40). Cowie BCC; Tadich A; Thomsen L; Garrett R; Gentle I; Nugent K; Wilkins S The Current Performance of the Wide Range (90–2500 EV) Soft X-Ray Beamline at the Australian Synchrotron. In AIP Conference Proceedings; 2010; Vol. 307, pp 307–310.

(41). Gann E; McNeill CR; Tadich A; Cowie BCC; Thomsen L Quick AS NEXAFS Tool (QANT): A Program for NEXAFS Loading and Analysis Developed at the Australian Synchrotron. J. Synchrotron Radiat 2016, 23 (1), 374–380. [PubMed: 26698087]

(42). Fredrickson GH The Equlibrium Theory of Inhomogenous Polymers; Oxford University Press, 2005.

(43). Hamersky MW; Smith SD; Gozen AO; Spontak RJ Phase Behavior of Triblock Copolymers Varying in Molecular Asymmetry. Phys. Rev. Lett 2005, 95 (16).

(44). Matsen MW Equilibrium Behavior of Asymmetric ABA Triblock Copolymer Melts. J. Chem. Phys 2000, 113 (13), 5539.

(45). Dura JA; Richter CA; Majkrzak CF; Nguyen NV Neutron Reflectometry, x-Ray Reflectometry, and Spectroscopic Ellipsometry Characterization of Thin SiO[Sub 2] on Si. Appl. Phys. Lett 1998, 73 (15), 2131.

(46). Winey KI; Thomas EL; Fetters LJ Swelling of Lamellar Diblock Copolymer by Homopolymer: Influences of Homopolymer Concentration and Molecular Weight. Macromolecules 1991, 24 (23), 6182–6188.

(47). Hashimoto T; Tanaka H; Hasegawa H Ordered Structure in Mixtures of a Block Copolymer and Homopolymers. 2. Effects of Molecular Weights of Homopolymers. Macromolecules 1990, 23 (20), 4378–4386.

(48). Chen S-C; Kuo S-W; Jeng U-S; Su C-J; Chang F-C On Modulating the Phase Behavior of Block Copolymer/Homopolymer Blends via Hydrogen Bonding. Macromolecules 2010, 43 (2), 1083–1092.

(49). Matsen MW; Thompson RB Equilibrium Behavior of Symmetric ABA Triblock Copolymer Melts. J. Chem. Phys 1999, 111 (15), 7139.

(50). Matsen MW Architectural Effect on the Surface Tension of an ABA Triblock Copolymer Melt. Macromolecules 2010, 43 (3), 1671–1674.

(51). Wignall GD; Ballard DGH; Schelten J Measurements of Persistence Length and Temperature Dependence of the Radius of Gyration in Bulk Atactic Polystyrene. Eur. Polym. J 1974, 10 (9), 861–865.

(52). Khoshkava V; Kamal MR Effect of Surface Energy on Dispersion and Mechanical Properties of Polymer/Nanocrystalline Cellulose Nanocomposites. Biomacromolecules 2013, 14 (9), 3155–3163. [PubMed: 23927495]

(53). Maher MJ; Self JL; Stasiak P; Blachut G; Ellison CJ; Matsen MW; Bates CM; Willson CG Structure, Stability, and Reorganization of 0.5 L 0 Topography in Block Copolymer Thin Films. ACS Nano 2016, 10 (11), 10152–10160. [PubMed: 27787994]

(54). Takano A; Kamaya I; Takahashi Y; Matsushita Y Effect of Loop/Bridge Conformation Ratio on Elastic Properties of the Sphere-Forming ABA Triblock Copolymers: Preparation of Samples and Determination of Loop/Bridge Ratio. Macromolecules 2005, 38 (23), 9718–9723.

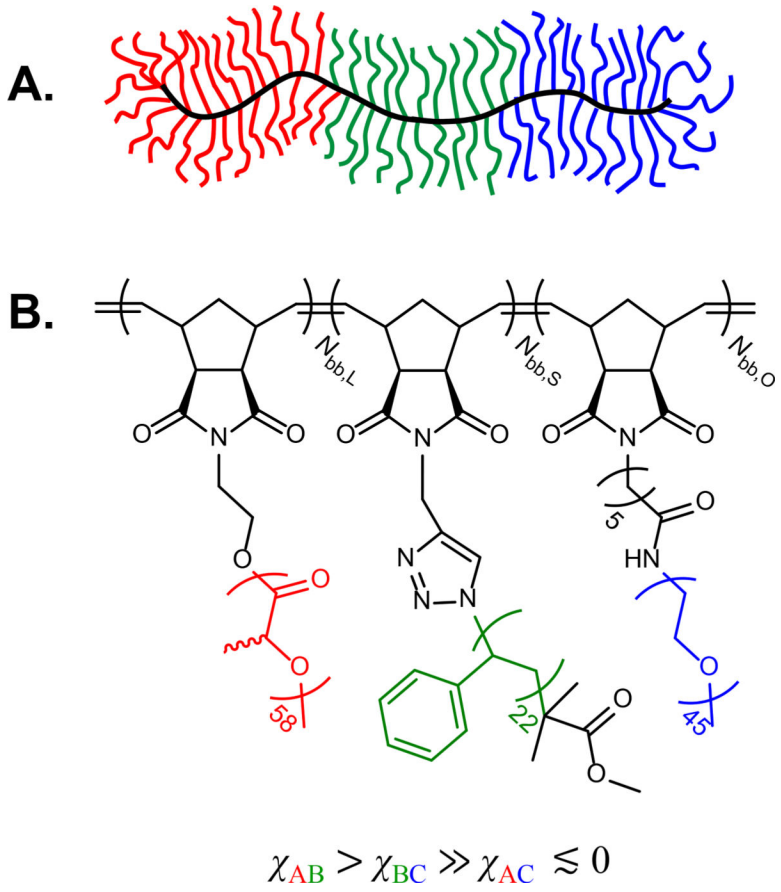

Figure 1.

(A) Illustration of the bottlebrush LSO triblock terpolymers studied herein. The polynorbornene backbone is indicated in black; the polylactide (L), polystyrene (S), and poly(ethylene oxide) (O) side chains are red, green, and blue, respectively. (B) Chemical structure of brush LSO.

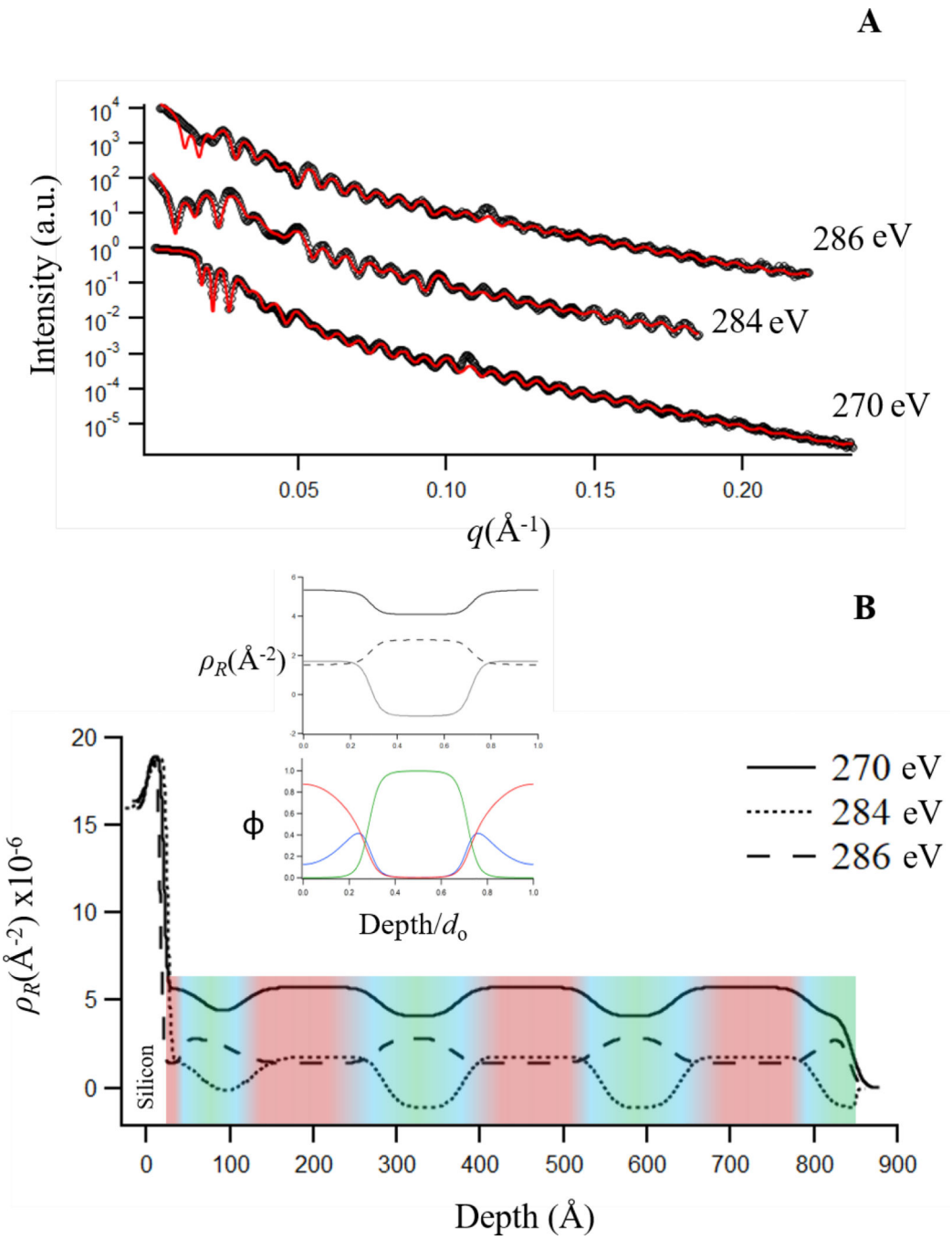

Figure 2:

A) Experimental (black circles) and simulated (red lines) reflectivity profiles collected for a brush LSO-12 thin film at three different energies. Simulated reflectivity profiles were calculated from the SLD profiles shown in part B. B) Composition profiles for LSO-12 determined from reflectivity measurements at 270 eV, 284 eV and 286 eV. The insets show the simulated SLD profile (top) and the composition profile calculated using SCFT (bottom), showing excellent qualitative agreement with the experimental results. The shaded

colors highlight the correspondence of each material to its SLD: PLA (*red*), PS (*green*), and PEO (*blue*).

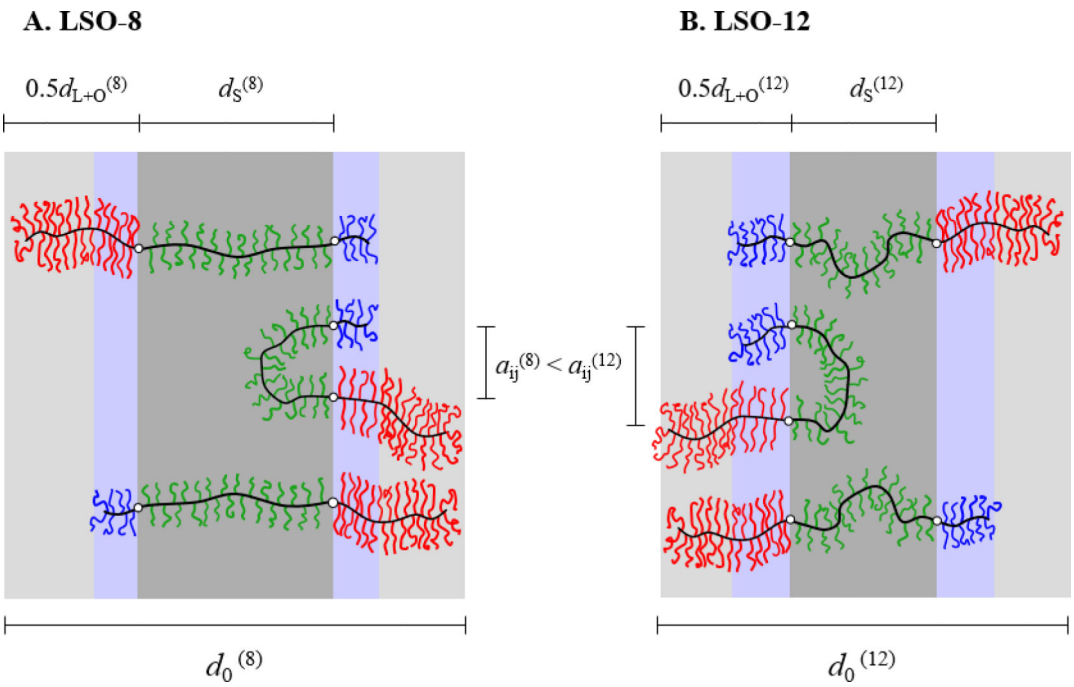

Figure 3:

Schematic illustration of chain configurations over one lamellar period (d_0) for (A) LSO-8 and (B) LSO-12. Relevant dimensions are indicated, including d_0, the thickness of the mixed PLA/PEO domains (d_{L+O}), the thickness of the PS domains (d_S), and the average distance between block junctions at the interface (a_{ij}). Note $d_0^{(8)} > d_0^{(12)}$ and $a_{ij}^{(8)} < a_{ij}^{(12)}$.

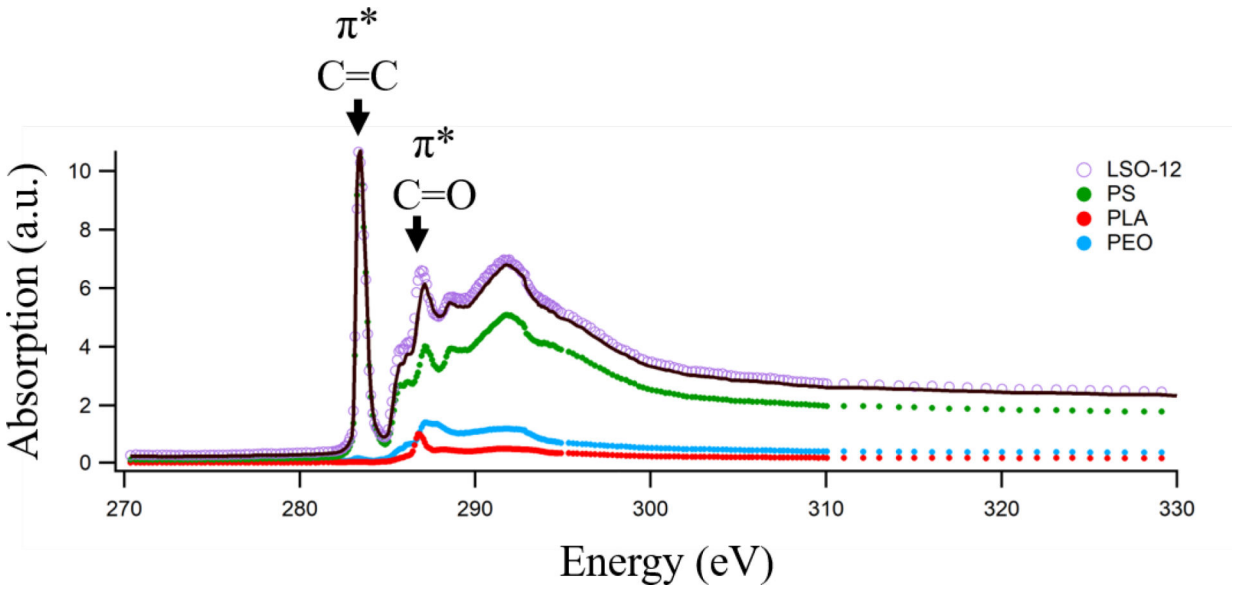

Figure 4:

NEXAFS analysis of LSO-12 at the carbon edge. Transitions corresponding to PS (C=C 1s→**π*** for the aromatic rings [284.5 eV]) and PLA (C=O 1s→**π*** for the carbonyl [288 eV]) are highlighted.

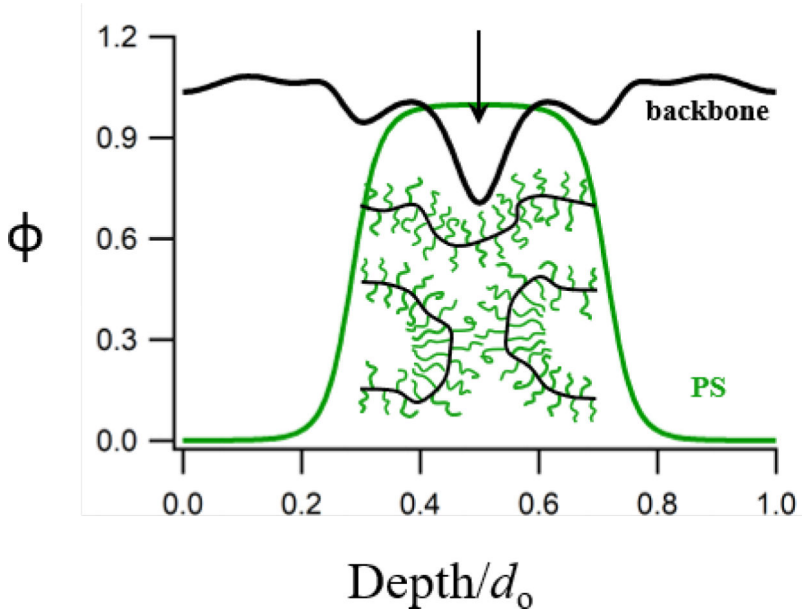

Figure 5:

SCFT composition profile for LSO-12 within one normalized lamellar period (z / d_0), where ϕ is the relative segment concentration. Calculated profiles for PS (*green*) and the backbone (*black*) are shown; PLA and PEO are not included. (See Figure 2 inset.) A schematic illustration of midblock configurations is provided. The arrow indicates a decrease in the backbone concentration at the center of the PS domain, suggesting a large fraction of looping midblocks.

Table 1.

Molecular characterization data for brush LSO triblock terpolymers.

Sample	$N_{bb,L}$ [a]	$N_{bb,S}$ [a]	$N_{bb,O}$ [a]	M_n (kg/mol)	$Đ$
LSO-8	26	24	8	197	1.00
LSO-12	26	24	12	206	1.01
LSO-16	26	24	16	215	1.07
LSO-20	26	24	20	224	1.00

[a]Number-average degree of polymerization through the backbone, determined from a combination of light scattering and ^{1}H NMR.

Table 2:

Dimensions resulting from best fits to the brush LSO reflectivity profiles. Uncertainties represent 95 % confidence intervals determined by the DREAM algorithm.[45]

Sample	d_0 (nm) (RSoXR)	d_0 (nm) SAXS[a]	d_{L+O} (nm)	d_S (nm)	Interfacial Width, w (nm)	PS Surface Thickness (nm)
LSO-8	26.1 ± 0.5	26.8	16.7 ± 0.3	9.4 ± 0.3	3.8 ± 0.5	4.6 ± 0.2
LSO-12	25.7 ± 0.6	25.2	16.9 ± 0.3	8.8 ± 0.3	4.5 ± 0.6	4.2 ± 0.3
LSO-16	25.2 ± 0.5	24.6	16.8 ± 0.2	8.4 ± 0.3	4.8 ± 0.8	3.8 ± 0.2
LSO-20	23.1 ± 0.5	23.6	16.6 ± 0.3	6.5 ± 0.2	7.5 ± 0.8	3.3 ± 0.2

[a]Lamellar period determined from previously reported hard SAXS measurements.[26]